

Generalizing thawing dark energy models: the standard vis-à-vis model independent diagnostics

DEBABRATA ADAK¹, DEBASISH MAJUMDAR² AND SUPRATIK PAL³

ABSTRACT

We propose a two parameter generalization for the dark energy equation of state (EOS) for thawing dark energy models, which includes PNgB, CPL and algebraic thawing models as limiting cases; and confront our model with latest Supernova Type Ia (SNe Ia) Data from Union 2.1 compilation, latest Observational Hubble Data (OHD), Cosmic Microwave Background (CMB) Data from 7 year WMAP results and latest Baryon Acoustic Oscillation Data from SDSS Data Release 9 to constrain our parameter space. The analysis reveals that thawing dark energy EOS is not unique from the observational point of view so far as the standard parameters (dark energy EOS, present value of matter density parameter and Hubble parameter) are concerned. In other words, different thawing dark energy models are not distinguishable from each other with the help of best-fit values of matter density parameter at present epoch, linear growth of matter perturbation and the average deceleration parameter. But tuning the model parameters does leave its impact on the variation of dark energy EOS as well as the model-independent parameters like the statefinder pair and $Om3$ parameters. We are thus led to the conclusion that unlike the standard parameters, the model-independent parameters and the variation of EOS serve as model discriminators for different thawing dark energy models.

1. Introduction

During the past two decades strong observational evidences have come out which have made late time acceleration of the universe almost a de facto phenomenon. These evidences have been brought forth *à la* independent astrophysical observations like Supernovae Type Ia (SNIa) luminosity distance modulus as a function of redshift (Amanullah et al. 2010; Davis et al. 2007; Kessler et al. 2009; Kowalski et al. 2008; Perlmutter et al. 1999; Riess et al. 1998; Riess et al. 2007;

¹Astroparticle Physics and Cosmology Division, Saha Institute of Nuclear Physics, 1/AF Bidhannagar, Kolkata 700064, India; debabrata.adak@saha.ac.in

²Astroparticle Physics and Cosmology Division, Saha Institute of Nuclear Physics, 1/AF Bidhannagar, Kolkata 700064, India; debasish.majumdar@saha.ac.in

³Physics and Applied Mathematics Unit, Indian Statistical Institute, 203 B.T.Road, Kolkata 700108, India; supratik@isical.ac.in

Riess et al. 2009; Suzuki et al. 2005; Wood-Vasey et al. 2007), Observational Hubble Data (OHD) (Gaztanaga et al. 2009; Jimenez et al. 2002; Simon et al. 2005; Zhang et al. 2012), Cosmic Microwave Background (CMB) Shift Parameter (Komatsu et al. 2009; Komatsu et al. 2011; Podariu et al. 2001; Ratra et al. 1999) and Baryon Acoustic Oscillation (BAO) Data (Percival et al. 2010; Sanchez et al. 2012; Samushia et al. 2009). Attempts have been made to explain accelerated expansion on the basis of existence of some exotic fluid, namely *dark energy*, in huge abundances in the universe. Though there exists a lot of dark energy models (see for example (Ali et al. 2010; Bento et al. 2003; Chen et al. 2011; Chen et al. 2011; Chiba et al. 2009; Bento et al. 2006; Dutta et al. 2011; Dutta et al. 2010; Dutta et al. 2009; Harko et al. 2010; Hirano et al. 2011; Kujat et al. 2006; Novosyadlyj et al. 2010) and references therein) that attempt to explain this accelerated expansion of the universe with standard as well as exotic ideas; the canonical and non-canonical scalar fields are the most promising candidates till date. Of late, Robert R. Caldwell and Eric V. Linder (Caldwell et al. 2005) categorized these scalar field models in two broad classes namely “freezing” and “thawing” dark energy, based on asymptotic behavior of the scalar field potential. In thawing models, dark energy equation of state w_X initially remains at -1 and deviates from -1 near present epoch whereas just the opposite behavior of w is witnessed in freezing models.

In thawing models deviation of w_X can lead to $w_X^0 > -1$ or $w_X^0 < -1$, where w_X^0 is value of w_X at present epoch. For slow-rolling quintessence scalar fields w_X moves to $w_X^0 > -1$, whereas for slow-rolling phantom scalar fields w_X becomes less than -1 at the present epoch. There are other works related to these slow-rolling scalar field thawing models (Dutta et al. 2009; Gupta et al. 2009; Sen et al. 2010; Scherrer et al. 2008; Scherrer et al. 2008) which lead to both quintessence and phantom behavior of w_X . In these slow-rolling scalar field models with nearly flat potential, initially the kinetic energy of the field is much smaller than the potential energy. This is because of the initial large Hubble damping which keeps the field nearly frozen at $w_X = -1$ at earlier era i.e., in radiation and matter dominated eras. Due to the expansion of the universe, energy density of the universe decreases. After the radiation and matter dominated eras, the field energy density becomes comparable to the background energy density of the universe resulting in the deviation of the field from its frozen state, thereby leading to deviation of w_X from -1 .

These slow-roll scalar field thawing models can be characterized by different relations between w_X and the scale factor a of the universe. Some typical examples include (Linder 2008) CPL parametrization (Eq. (1)), PGNB models (Eq. (2)) and algebraic thawing model (Eq. (3)). The corresponding equation of state parameterizations are given by,

$$\frac{dw_X}{d(\ln a)} = (1 + w_X) \quad (1)$$

$$\frac{dw_X}{d(\ln a)} = F(1 + w_X) \quad (2)$$

$$\frac{dw_X}{d(\ln a)} = (1 + w_X) \left(3 - \frac{3-p}{1+ba^{-3}} \right), \quad (3)$$

where F is a parameter which is inversely proportional to the symmetry breaking energy scale and p and b are two free parameters.

In this work, we propose a two parameter generalization for this thawing dark energy models as

$$\frac{dw_X}{da} = (1 + w_X)f(a) \quad (4)$$

where $f(a)$ is an arbitrary function of scale factor a . In this paper, we have chosen $f(a)$ as $f(a) = c/a^n$, where c and n are two otherwise arbitrary parameters. With $n = 1$ and $c = 1$ our proposal exactly overlaps with CPL thawing dark energy model (Linder 2008). For $n = 1$ and $1 < c < 3$, our proposal leads to PNGB thawing dark energy model (Linder 2008). PNGB dark energy model is studied exclusively for scalar fields dark energy with PNGB potential (Dutta et al. 2007; Frieman et al. 1995; Kaloper et al. 2006; Rosenfeld et al. 2007). For suitable choice of the parameters n and c , our model can approximately reflect algebraic thawing as well. As it turns out, all the existing (and probably, upcoming) thawing dark energy models fall in this broad parametrization with different values of the parameters n and c . So, rather than proposing individual models, it is quite reasonable to construct a generic form of parametrization, analyze it and search for possible constraints on the parameters from observations. This is the primary objective of the present article.

We also draw some comparisons among the results obtained for different values of n (i.e., for $n = 1$, $n = 1.5$ and $n = 2$) with different fixed values of c and vice-versa. We further provide justification for this proposed generalized form of thawing dark energy model against the other existing models by comparing them with ours. Moreover, we constrain our model by latest Supernova Type Ia Data from Union2.1 compilation (Amanullah et al. 2010; Davis et al. 2007; Kessler et al. 2009; Kowalski et al. 2008; Perlmutter et al. 1999; Riess et al. 1998; Riess et al. 2007; Riess et al. 2009; Suzuki et al. 2005; Wood-Vasey et al. 2007), newly released Observational Hubble parameter Data (Gaztanaga et al. 2009; Jimenez et al. 2002; Simon et al. 2005; Zhang et al. 2012), Cosmic Microwave Background Shift Parameter Data from WMAP7 year results (Komatsu et al. 2009; Komatsu et al. 2011; Podariu et al. 2001; Ratra et al. 1999) and the latest Baryon Acoustic Oscillation Data from SDSS Data Release 9 (Percival et al. 2010; Sanchez et al. 2012; Samushia et al. 2009). For such analyses we have five parameters in total namely c , n , w_X^0 , Ω_m^0 and H_0 (where Ω_m^0 and H_0 are matter density at present epoch normalized to critical density and Hubble parameter at present epoch respectively). Since the value of Ω_r^0 (the normalized radiation density at present epoch) is very low we do not treat it as a parameter and consider $\Omega_r^0 = 5.05 \times 10^{-5}$ (Beringer et al. 2012) for numericals. Our analysis also helps in comparing the standard diagnostics with model independent ones, and reveals the pros and cons of each one.

The major conclusions of the paper are as follows:

1. Results obtained for different n values (with different values of c) barely differ from the observational point of view. In other words we can say that values of n (with different values of c) can hardly affect the matter density parameter Ω_m^0 , average deceleration parameter q_{av}

and the growth of matter perturbation f . Therefore it is difficult to provide a unique dark energy EOS w_X for the thawing dark energy models as different values of n with different values of c lead to the same cosmological dynamics.

2. Though the equation of state parameter does not leave trace on model discrimination for thawing dark energy, values of n and c can be constrained by $w_X - w'_X$ ($w'_X = \frac{dw_X}{d\ln(a)}$) plots (Caldwell et al. 2005) for thawing dark energy models. More importantly, $w_X - w'_X$ plots can also serve as a model discriminator for the thawing dark energy models. The non-linear $w_X - w'_X$ plots can be realized for values of n other than 1 with different values of c . This is an important issue as PNGB and CPL parameterizations can result in linear $w_X - w'_X$ plots.
3. Most importantly, the model-independent parameters like statefinder pair $\{r, s\}$ and the so called $Om3$ parameter do play a crucial role in discriminating among different thawing dark energy models. Therefore, unlike the standard parameters mentioned in Item 1, these parameters indeed serve as model discriminators for different thawing dark energy models.

2. The scheme of generalization

2.1. Generalized thawing dark energy EOS

We propose a minimal two parameter generalization for thawing dark energy EOS w_X as,

$$\frac{dw_X}{da} = (1 + w_X)f(a) \quad (5)$$

where $f(a)$ is an arbitrary function of scale factor a of the universe. We study the dynamical universe with radiation, matter and thawing dark energy obeying our proposed EOS w_X with $f(a) = \frac{c}{a^n}$. Our choice of $f(a)$ for generalized thawing model is motivated by the following findings:

- i) for $n = 1$ and $c = 1$, our model is exactly same as CPL parametrization (Eq 1).
- ii) for $n = 1$ and $c = F$, our model is exactly same as PNGB model (Eq 2).
- iii) algebraic thawing case (Eq 3) can approximately be obtained for certain choice of c and n in terms of b and p .
- iv) for any higher values of n , generalized thawing dark energy EOS takes the form

$$w_X(a) = -1 + (1 + w_X^0) \exp \left[\frac{c}{(n-1)} (1 - a^{(1-n)}) \right] \quad (6)$$

where w_X^0 is the value of w_X at the present epoch. Expansion of $w_X(a)$ about $a = 1$ gives,

$$w_X(a) = w_X^0 - c(1 + w_X^0)(1 - a) + \frac{1}{2}(1 + w_X^0)(c^2 - cn)(1 - a)^2 + \text{higher order terms} . \quad (7)$$

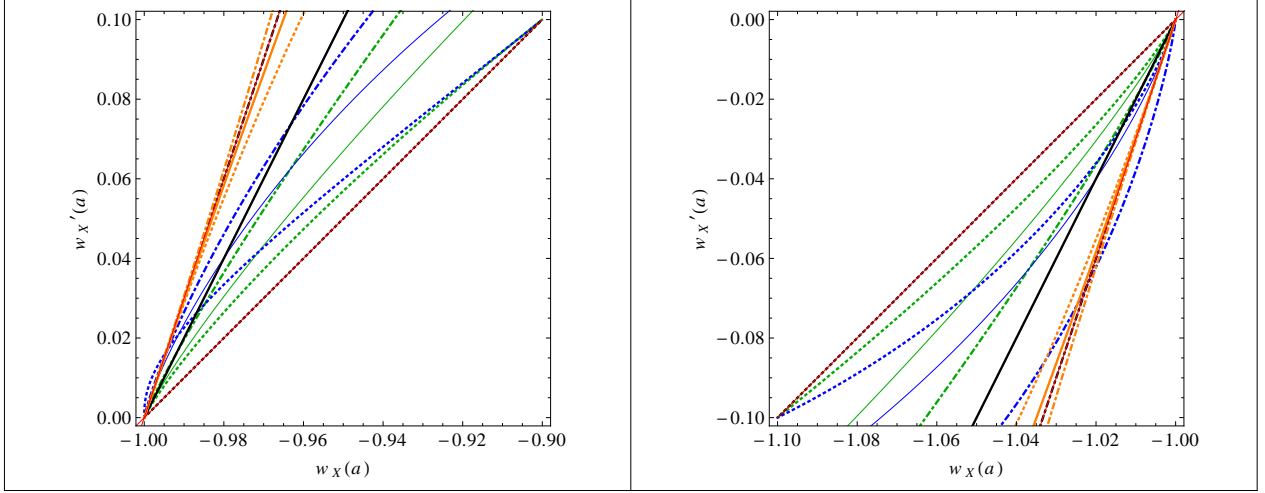


Fig. 1.— The left fig. is for $w_X^0 = -0.9$ and the right fig. corresponds to $w_X^0 = -1.1$. Black and orange plots are for PNGB and algebraic thawing models for $w_X^0 = -0.9$. The dotted, solid and dot-dashed lines are for $F = 1, 2, 3$ in the PNGB thawing case and for algebraic thawing case they are for $p = b = 1$, $p = b = 2$ and $p = b = 6$. The blue and green curves are for our generalized thawing EOS. Green (dotted, solid, dot-dashed) lines are for $n = 1.2$ ($c = 1, 1.2, 1.5$). Similarly blue (dotted, solid, dot-dashed) lines are for $n = 1.5$ ($c = 1, 1.2, 1.5$). The area between solid red lines is the allowed thawing region (Caldwell et al. 2005).

In order to test the validity of our generalized model we show in Fig. 1, the theoretically predicted $w_X - w'_X$ ($w'_X = \frac{dw_X}{d\ln(a)}$) plots for different thawing models that arise for different values of n and c (we will compare it with direct observational data later in this paper). We find from Fig. 1, theoretically obtained $w_X - w'_X$ plane for different combinations of c and n in our model satisfy the allowed regions for the same (Caldwell et al. 2005). In Fig. 1, the left plot is for quintessential thawing with $w_X^0 = -0.9$ and the right one is for the case of thawing originated in phantom scenarios with $w_X^0 = -1.1$. For $n = 1$ with $c = 1$ (dotted) we get CPL thawing (Eq. (1)) and for $n = 1$ with $c = 2, 3$ (solid and dot-dashed respectively) we get PNGB thawing (Eq. (2)). The plots in black in Fig. 1 indicate these two models in the $w_X - w'_X$ plane. The orange plots are for the algebraic thawing model with $p = b = 1$ (dotted lines), $p = b = 2$ (solid lines) and $p = b = 6$ (dot-dashed lines). The results with higher values of n are shown by the green ($n = 1.2$) and blue plots ($n = 1.5$). The dotted, solid and dot-dashed lines in this case corresponds to $c = 1, 1.2, 1.5$ respectively.

2.2. The standard and model independent parameters

As is well-known, any dark energy model must at least probe three parameters directly from observations:

- i) the present value of equation of state for dark energy (ω_X^0)
- ii) the present value of matter density (Ω_M^0)
- iii) the Hubble parameter today (H_0).

Nevertheless, dark energy model building today is tightly constrained by several observations, which, taken together, leave out a very narrow window through which the model should pass. So, from today's perspectives, apart from the above three good old parameters, the supplementary parameters which one needs to address are the following:

The statefinder $\{r, s\}$ (Sahni et al. 2002) serves as a geometrical diagnostic to probe the properties of dark energy in a model independent manner. This pair $\{r, s\}$ has been studied extensively in the earlier works (TsujiKawa 2010; Ali et al. 2010; Das et al. 2011; Li et al. 2009; Panotopoulos 2008). For the late universe ($z < 10^4$), which is well approximated by the presence of matter and dark energy, the statefinder pair $\{r, s\}$ can be expressed as,

$$r = 1 + \frac{9}{2}\Omega_X w_X(1 + w_X) - \frac{3}{2}\Omega_X \frac{\dot{w}_X}{H}, \quad (8)$$

$$= 1 + \frac{9}{2}\Omega_X w_X(1 + w_X) - \frac{3}{2}a\Omega_X \frac{dw_X}{da}, \quad (9)$$

$$s = 1 + w_X - \frac{1}{3} \frac{\dot{w}_X}{w_X H}, \quad (10)$$

$$= 1 + w_X - \frac{1}{3} \frac{a}{w_X} \frac{dw_X}{da}. \quad (11)$$

where a is the scale factor of the universe and Ω_X is the dark energy density parameter and dot represents the derivative with respect to cosmic time t . In the late universe we have $\Omega_m + \Omega_X = 1$, Ω_m being the matter density parameter. For Λ CDM model, it can be checked that the statefinder pair $\{r, s\}$ takes the value $r = 1$ and $s = 0$. Any deviation in r from 1 and s from 0, indicates the existence of varying dark energy model in the universe.

The Om parameter proposed by Sahni et al. (Sahni et al. 2008), is another tool to distinguish the dynamical dark energy from the cosmological constant. The uncertainty in matter density parameter allows significant errors in cosmological reconstructions of dark energy. Om parameter can in practice differentiate between the models, independent of the matter density parameter. The Om diagnostic has been studied well in the earlier works (Sahni et al. 2008; Nesseris et al. 2010; Shafieloo et al. 2012; Huang et al. 2011; Shafieloo et al. 2010; Lu et al. 2008). Om parameter is defined in terms of Hubble parameter which can directly be measured in cosmological observations. The two-point Om diagnostic is given by,

$$Om(z_2; z_1) = \frac{h^2(z_2) - h^2(z_1)}{(1 + z_2)^3 - (1 + z_1)^3}, \quad (12)$$

where $h(z) = H(z)/H_0$.

It can be easily seen that for cosmological constant $Om(z_1, z_2) = 0$ and when $z_1 < z_2$, $Om(z_1, z_2) > 0$ ($Om(z_1, z_2) < 0$) represents the case of quintessence (phantom) (Sahni et al. 2008).

This is how Om evaluated at two different redshifts (z_1 and z_2) can help in distinguishing the dark energy model. Needless to mention that this procedure is independent of Ω_m^0 and H_0 . The three-point diagnostic $Om3$ is defined by,

$$Om3(z_1, z_2, z_3) = \frac{Om(z_2; z_1)}{Om(z_3; z_1)}. \quad (13)$$

For Λ CDM model $Om3 = 1$.

Another dimensionless parameter, which is useful for determining the beginning of cosmic acceleration in dark energy model, is the average deceleration parameter q_{av} , defined as (Sahni et al. 2008),

$$q_{av} = \frac{1}{(t_2 - t_1)} \int_{t_2}^{t_1} q(t) dt. \quad (14)$$

We use Eqs. (9, 11, 13, 14) for evaluating the statefinder pair $\{r, s\}$, $Om3$ and q_{av} for the case of our generalization of thawing dark energy model.

Further more, galaxy cluster formation is not directly influenced by the existence of dark energy. The presence of dark energy alters the Hubble expansion rate which affects the growth of inhomogeneities in the cold matter sector. In the linear regime of matter perturbations, the evolution of the inhomogeneities are governed by the relation (Wang et al. 1998)

$$\frac{d^2 \ln \delta}{d(\ln a)^2} + \left(\frac{d \ln \delta}{d \ln a} \right)^2 + \frac{1}{2} \left(\frac{d \ln \delta}{d \ln a} \right) (1 - 3w_X(1 - \Omega_m)) = \frac{3}{2} \Omega_m \quad (15)$$

where the matter density contrast $\delta = \delta \rho_m / \rho_m$ with ρ_m the matter density. The growth factor f is defined by (Wang et al. 1998),

$$f = \frac{d \ln \delta}{d \ln a} \quad (16)$$

Eq. (15) can be written in terms of growth factor f (defined in Eq. (16)) as,

$$\frac{df}{d \ln a} + f^2 + \frac{1}{2} f (1 - 3w_X(1 - \Omega_m)) = \frac{3}{2} \Omega_m. \quad (17)$$

The growth equation can be expressed in terms of the redshift z by the relation $\ln a = -\ln(1+z)$. The growth factor is well approximated by the ansatz (Wang et al. 1998)

$$f = \Omega_m(z)^\gamma \quad (18)$$

where γ is termed as "growth index". This quantity is affected by dark energy models via $\Omega_m(z)$.

3. Compilation of combined datasets

For the purpose of putting constraints on the generalized thawing dark EOS, we use the latest Supernova Type Ia (SNe Ia) Data from the Union 2.1 compilation (Amanullah et al. 2010; Davis et al. 2007; Kessler et al. 2009; Kowalski et al. 2008; Perlmutter et al. 1999; Riess et al. 1998; Riess et al. 2007; Riess et al. 2009; Suzuki et al. 2005; Wood-Vasey et al. 2007), Observational Hubble Data (OHD) (Gaztanaga et al. 2009; Jimenez et al. 2002; Simon et al. 2005; Zhang et al. 2012), Cosmic Microwave Background Data (CMB) from 7 year WMAP results (Komatsu et al. 2009; Komatsu et al. 2011; Podariu et al. 2001; Ratra et al. 1999), and Baryon Acoustic Oscillation (BAO) Data from SDSS Data Release 9 (Percival et al. 2010; Sanchez et al. 2012; Samushia et al. 2009). There are a total of 607 data points (580 data point from SNe Ia, 25 from OHD, and 1 each from CMB and BAO). We make a combined χ^2 analyses of the data sets comprising of all 607 data points to constrain our model parameters w_X^0 , Ω_m^0 and H_0 , as well as to confront with the model-independent parameters mentioned in Section 2. This makes our analysis robust.

3.1. Union 2.1 compilation of Supernova Type Ia Data

Luminosity distance (d_L) measurement of distant supernovae with redshifts z is the first observational data to probe the current acceleration of the universe and the dark energy properties as well. The most recent compilation of the Supernova Type Ia Data is given by Union 2.1 dataset. The data is tabulated in terms of distance modulus $\mu(z)$ with redshift z . The distance modulus can be written as

$$\mu(z) = 5 \log_{10}(D_L(z)) + \mu_0 , \quad (19)$$

where $D_L(z) = H_0 d_L(z)/c$, c being the speed of light and $\mu_0 = 42.38 - 5 \log_{10} h$ with h given by $H_0 = 100h \text{ KmSec}^{-1} \text{ Mpc}^{-1}$.

χ^2 of SNe Ia data is given by,

$$\chi_{\text{SN}}^2(w_X^0, \Omega_m^0, H_0) = \sum_i \left[\frac{\mu_{\text{obs}}(z_i) - \mu(z_i; w_X^0, \Omega_m^0, H_0)}{\sigma_i} \right]^2 , \quad (20)$$

Marginalizing over the nuisance parameter μ_0 , one gets the χ^2 as,

$$\chi_{\text{SN}}^2(w_X^0, \Omega_m^0) = A - B^2/C , \quad (21)$$

where A , B and C are given by,

$$\begin{aligned} A &= \sum_i \left[\frac{\mu_{\text{obs}}(z_i) - \mu(z_i; w_X^0, \Omega_m^0, \mu_0 = 0)}{\sigma_i} \right]^2 \\ B &= \sum_i \left[\frac{\mu_{\text{obs}}(z_i) - \mu(z_i; w_X^0, \Omega_m^0, \mu_0 = 0)}{\sigma_i} \right] \end{aligned}$$

$$C = \sum_i \frac{1}{\sigma_i^2} \quad (22)$$

3.2. Observational Hubble Data (OHD)

Measurements of Hubble parameters from differential ages of galaxies provide another way to probe the late time acceleration of the expanding universe. Gemini Deep Deep Survey GDDS (Abraham et al. 2004), SPICES and VVDS surveys provide the values of the Hubble parameter at 15 different redshift values and with the data release 9 from Sloan Digital Sky Survey (SDSS) we have a total of 25 data points at present (Gaztanaga et al. 2009; Jimenez et al. 2002; Simon et al. 2005; Zhang et al. 2012). The χ^2 function for the analysis of this observational Hubble data can be defined as

$$\chi_{\text{OHD}}^2(w_X^0, \Omega_m^0, H_0) = \sum_{i=1}^{15} \left[\frac{H_{\text{obs}}(z_i) - H(z_i; w_X^0, \Omega_m^0, H_0)}{\sigma_i} \right]^2. \quad (23)$$

The latest data release for the variation of Hubble parameter with redshift has been listed in Table 1.

3.3. CMB Shift Parameter Data

CMB shift parameter R , to a great extent, is a model independent quantity extracted from CMB power spectrum. It is given by

$$R(z_*) = (\Omega_m H_0^2)^{1/2} \int_0^{z_*} dz / H(z) \quad (24)$$

where z_* is the redshift value at the time when photons decoupled from matter in the universe. z_* can be calculated as (with Ω_b being the baryon density parameter)

$$z_* = 1048[1 + 0.00124(\Omega_b h^2)^{-0.738}[1 + g_1(\Omega_m h^2)^{g_2}], \quad (25)$$

where the functions g_1 and g_2 read as

$$g_1 = 0.0783(\Omega_b h^2)^{-0.238}(1 + 39.5(\Omega_b h^2)^{-0.763})^{-1}, \quad (26)$$

$$g_2 = 0.560(1 + 21.1(\Omega_b h^2)^{1.81})^{-1}. \quad (27)$$

$$\chi_{\text{CMB}}^2(w_X^0, \Omega_m^0, H_0) = \left[\frac{R(z_*, w_X^0, \Omega_m^0, H_0) - R}{\sigma_R} \right]^2. \quad (28)$$

From WMAP 7 year data (Komatsu et al. 2009; Komatsu et al. 2011; Podariu et al. 2001; Ratra et al. 1999) we get $R = 1.715 \pm 0.021$.

3.4. Baryon Acoustic Oscillation Data

Baryon Acoustic Oscillation or BAO (observed in the matter power spectrum) is the consequence of the primordial fluctuations frozen in the large scale structure after the recombination is reached. The acoustic peak in the two-point galaxy correlation function was first detected by the SDSS by observing the galaxy distribution in the sky and a preferred comoving scale r_s , at redshift $z = 0.35$, was measured.

The dimensionless combination $A(z) = D_V(z)\sqrt{\Omega_m^0 H_0^2}/z$ is independent of H_0 and is well constrained by the present SDSS data. We use the measured value of $A(z)$ at $z = 0.57$ ($A_{\text{obs}}(0.57) = 0.444 \pm 0.014$ (Percival et al. 2010; Sanchez et al. 2012; Samushia et al. 2009)) to constrain our model parameter space.

The χ^2 for the BAO data is defined as

$$\chi_{\text{BAO}}^2(w_X^0, \Omega_m^0) = \frac{[A_{\text{obs}}(0.57) - A(0.57, w_X^0, \Omega_m^0)]^2}{0.016^2}. \quad (29)$$

3.5. Combined χ^2 analyses

Combining all the datasets from Sections (3.1) - (3.4), comprising of altogether 607 data points, the combined χ^2 can be evaluated as:

$$\chi^2(w_X^0, \Omega_m^0, H_0) = \chi_{\text{SN}}^2(w_X^0, \Omega_m^0) + \chi_{\text{OHD}}^2(w_X^0, \Omega_m^0, H_0) + \chi_{\text{CMB}}^2(w_X^0, \Omega_m^0, H_0) + \chi_{\text{BAO}}^2(w_X^0, \Omega_m^0).$$

In what follows, we minimize this combined χ^2 with the observational data sets and search for possible consequences by confronting our generalized model directly with observations.

4. Data analysis and results

In this section our primary target is to make a combined χ^2 analysis for our generalized model as proposed in Eq (4) with the SNe Ia, OHD, CMB and BAO data for evaluating the parameters space and their 1σ and 2σ confidence level (C.L.) limits. We further study these cases to compare between the results for $n = 1$ and other values of n with the different values of c . Our results are tabulated in Table 2, 3 and 4. There are five parameters in this generalized thawing model and they are n , c , w_X^0 , Ω_m^0 and H_0 . We fix the values of n at 1, 1.5, 2 with different values of c so that we can compare different thawing models and find the best fit values of other three parameters by χ^2 analyses. The results of χ^2 analyses for PNGB and CPL models are furnished as Case I below and the χ^2 analyses results for the thawing models with $n = 1.5$ and $n = 2$ are given as Case II and Case III respectively.

4.1. Standard parameters for different values of n and c

Case I: $n = 1$ (CPL & PANGB)

The χ^2 analyses results for $n = 1$ with different values of c are tabulated in the Table 2. These are the cases of PANGB and CPL ($c = 1$) thawing dark energy models. Here we choose the values of c to be 1, 1.5, 2. It is seen from Table 2 that with the increases of the value of parameter c , the thawing dark energy EOS transcends from quintessence to phantom domain via cosmological constant. During this course of change of EOS (w_X), the value of matter density parameter at present epoch remains unaltered and present epoch value of the Hubble parameter barely suffers any change in its magnitude. Also needless to mention here that the value of total χ^2 remains unchanged as is evident from Table 2.

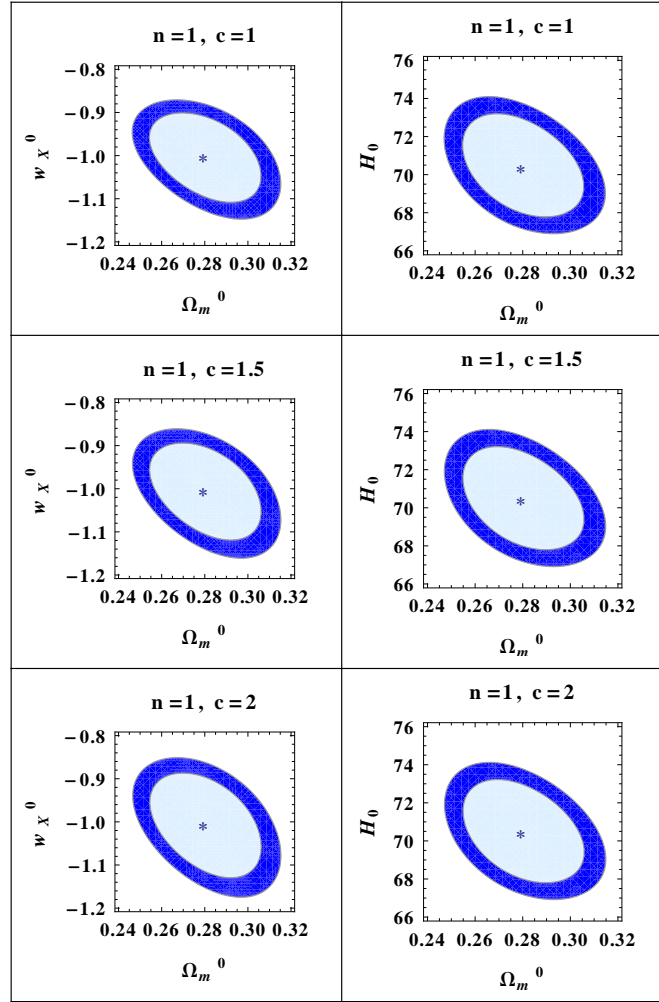


Fig. 2.— This Fig shows the contours for $n = 1$. χ^2 minimization gives the best fit values which are marked as * in the plot.

In Fig. 2, the 1σ and 2σ contours for $n = 1$ with different values of c are shown by light blue and dark blue shaded regions respectively. The “*” in the plots represents the best fit values obtained by χ^2 minimization (Table 2).

Case II: $n = 1.5$

The χ^2 minimization results obtained for $n = 1.5$ with $c = 0.5, 1, 1.5$ are tabulated in Table 3. Here also the best fit results suggest a phase transition from quintessence to phantom nature of thawing dark energy EOS as c increases. But the best fit values of present epoch matter density parameter Ω_m^0 remain unchanged. Also one observes that the best fit values of the Hubble parameters H_0 at the present epoch are hardly changed in these cases.

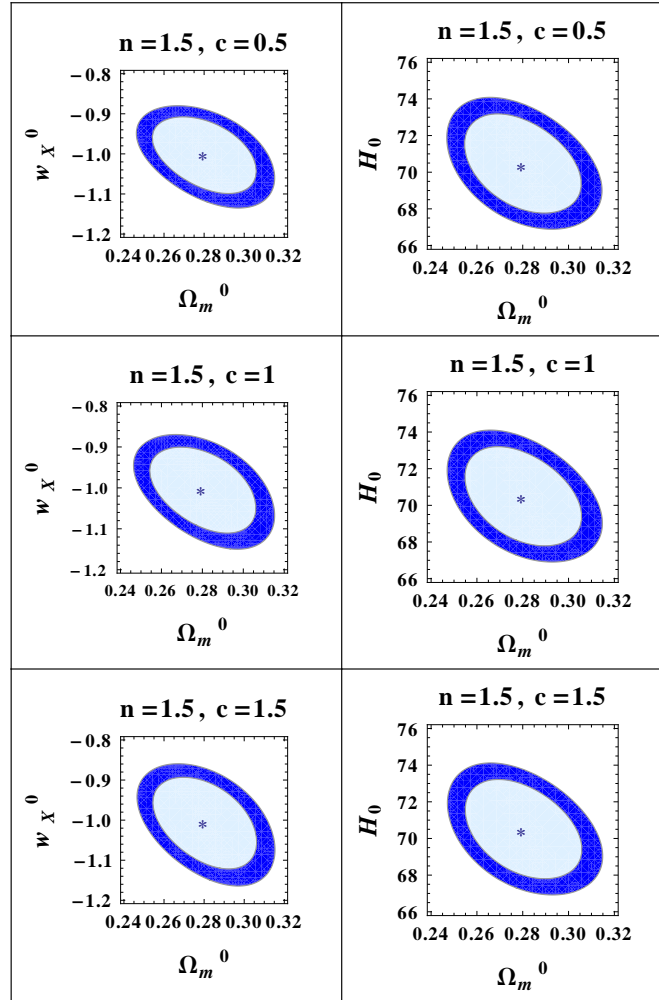


Fig. 3.— This Fig shows the contours for $n = 1.5$. χ^2 minimization gives the best fit values which are marked as * in the plot.

In Fig. 3, the best fit values (obtained from χ^2 minimization) are shown with “*” symbol and

the 1σ and 2σ contours are given by light blue and dark blue color shadings.

Case III: $n = 2$

The results for $n = 2$ with $c = 0.5, 1, 1.5$ are tabulated in Table 4. Like the previous two cases discussed above, here also one can see the transition from quintessence to phantom behavior of thawing dark energy EOS with no change in the present epoch value of matter density parameter Ω_m^0 with the increasing value of c . the present epoch value of the Hubble parameter also barely changes.

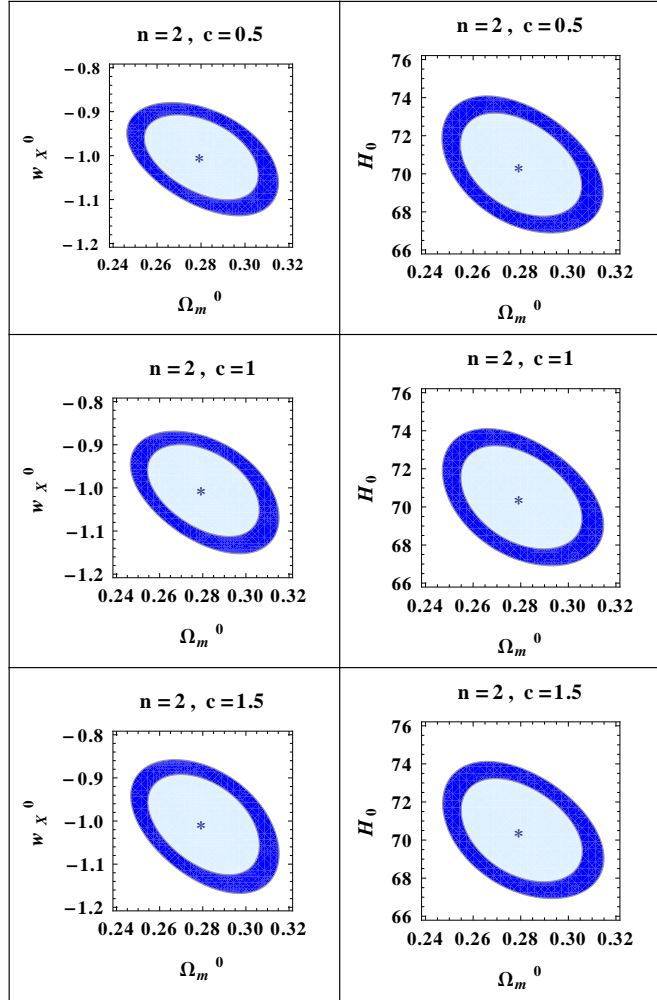


Fig. 4.— This Fig shows the contours for $n = 2$. χ^2 minimization gives the best fit values which are marked as * in the plot.

As in the previous two occasions, best fit values and 1σ , 2σ contours (obtained from χ^2 minimization) is denoted by “*” and light blue, dark blue color shades respectively in Fig. 4.

Now we compare different values of n for a particular value of c . For $c = 1$, one can figure out from the Tables 2, 3, 4 that as n value increases from 1 to 2, w_X^0 shifts from -0.9992 to -1.0008 indicating the phase transition from quintessence to phantom nature of thawing. The present value of matter density parameter Ω_m^0 remains unchanged and the present value of Hubble parameter H_0 hardly suffers any change in these cases. The same analogy goes for $c = 1.5$ case.

In Fig. 5, the growth of matter perturbation is plotted against redshift z . The upper (lower) panel is for $f(N = -7) = 0.8$ ($f(N = 7) = -0.9$). The growth of matter perturbation is identical in all the cases suggesting the formation of the same large scale structure in all cases of thawing considered here (i.e., for $n = 1$, $n = 1.5$ and $n = 2$). Therefore the growth factor f does not serve as a model discriminator but acts as a supplementary probe to confirm correct estimation of cosmic structures formed.

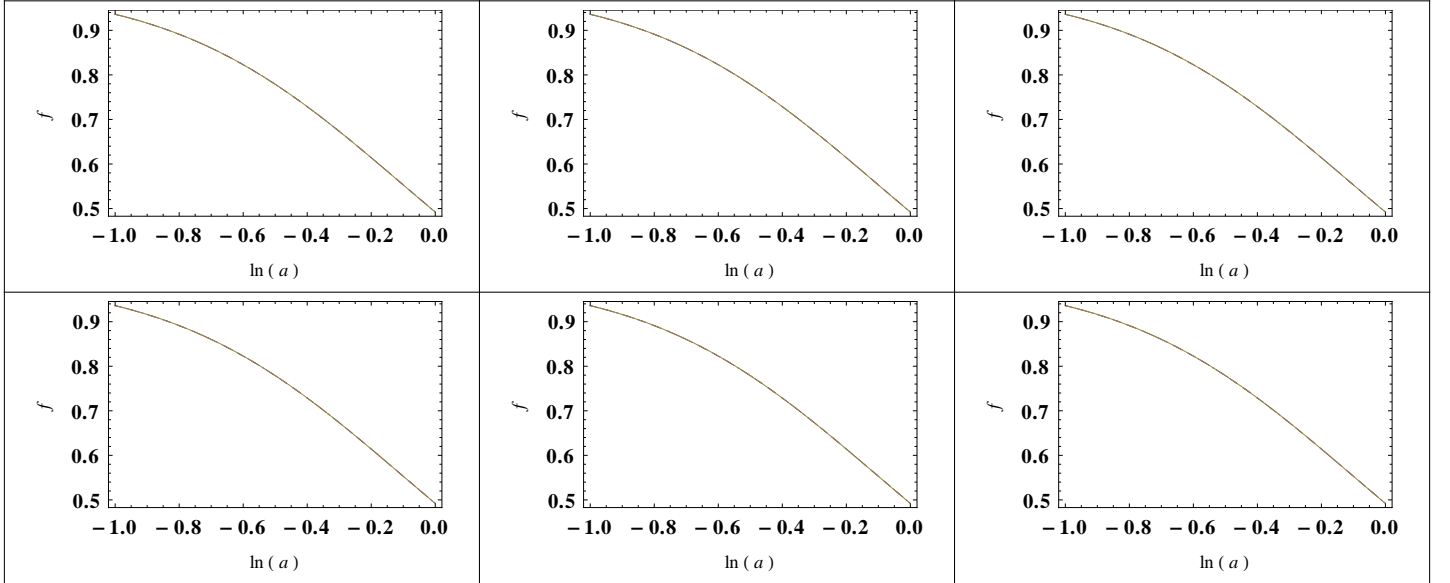


Fig. 5.— Variation of the growth factor with logarithm of scale factor. The upper (lower) three plots are for $f(N = -7) = 0.8$ ($f(N = -7) = 0.9$) where $N = \ln a$ is the number of e -foldings. Each plot actually depicts 3 different plots overlapping with each other: for $n = 1$ with $c = 1, 1.5, 2$ and for $n = 1.5, n = 2$ they are for $c = 0.5, 1, 1.5$.

Fig 6 depicts variation of w'_X with w_X as obtained by directly using observational data from the combined dataset. The plots show that we indeed have non-linear behavior for the generalized thawing dark energy model from observations. Comparison of these plots with our theoretical predictions, as done in Fig 1 will be interesting. So, Fig 6 goes over Fig 1 which was only a theoretical prediction. As it turns out from this figure, the variation of the equation of state indeed serves as a model-discriminator for different thawing dark energy models.

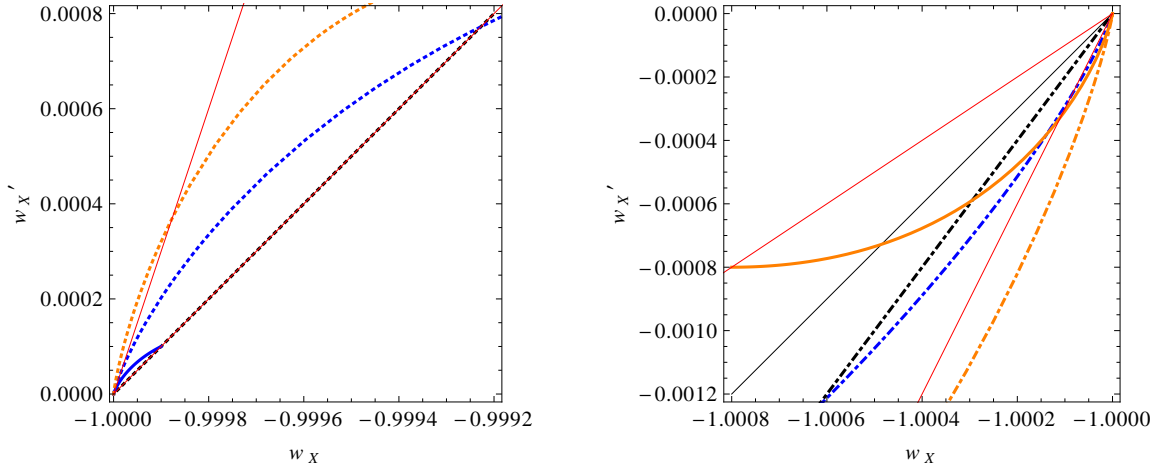


Fig. 6.— The left plot is for $w_X^0 > -1$ and the right plot is for $w_X^0 < -1$. In both the figs, the blue lines are for $n = 1.5$, the orange line are for $n = 2$ and the black lines corresponds to $n = 1$. The dotted, solid and dotdashed lines corresponds to $c = 1$, $c = 1.5$, $c = 2$ for the case of $n = 1$ and $c = 0.5$, $c = 1$, $c = 1.5$ for the case of $n = 1.5$ and $n = 2$.

z	$H(z)$ (Km. s ⁻¹ . Mpc ⁻¹)	σ_H (Km. s ⁻¹ . Mpc ⁻¹)
0.090	69	12
0.170	83	8
0.270	77	14
0.400	95	17
0.900	117	23
1.300	168	17
1.430	177	18
1.530	140	14
1.750	202	40
0.480	97	62
0.880	90	40
0.179	75	4
0.199	75	5
0.352	83	14
0.593	104	13
0.680	92	8
0.781	105	12
0.875	125	17
1.037	154	20
0.24	79.69	3.32
0.43	86.45	3.27
0.07	69.0	19.6
0.12	68.6	26.2
0.20	72.9	29.6
0.28	88.8	36.6

Table 1: Hubble parameter ($H(z)$) versus redshift (z) data from (Gaztanaga et al. 2009; Jimenez et al. 2002; Simon et al. 2005; Zhang et al. 2012) . Where $H(z)$ and σ_H are in km s⁻¹ Mpc⁻¹.

n	c	best-fit values of (w_0, Ω_m^0, H_0)	Minimum value of χ^2
1	1	(-0.9992, 0.279, 70.47)	576.26
1	1.5	(-1.0008, 0.279, 70.49)	576.26
1	2	(-1.0023, 0.279, 70.50)	576.26

Table 2: Best-fit values of parameters and minimum values of χ^2 from combined χ^2 analyses of SNIa, CMB, OHD and BAO data for Case I.

n	c	best-fit values of (w_0, Ω_m^0, H_0)	Minimum value of χ^2
1.5	0.5	(-0.9979, 0.279, 70.46)	576.26
1.5	1	(-0.9999, 0.279, 70.48)	576.26
1.5	1.5	(-1.0017, 0.279, 70.49)	576.26

Table 3: Best-fit values of parameters and minimum values of χ^2 from combined χ^2 analyses of SNIa, CMB, OHD and BAO data for Case II.

n	c	best-fit values of (w_0, Ω_m^0, H_0)	Minimum value of χ^2
2	0.5	(-0.9985, 0.279, 70.47)	576.26
2	1	(-1.0008, 0.279, 70.49)	576.26
2	1.5	(-1.0027, 0.279, 70.50)	576.26

Table 4: Best-fit values of parameters and minimum values of χ^2 from combined χ^2 analyses of SNIa, CMB and OHD and BAO data for Case III.

4.2. Model-independent diagnostics

In Fig. 7 we show the variation of the statefinder parameters $\{r, s\}$ with redshift z for $n = 1$ case which is known as CPL for $c = 1$ or PANGB for other values of c . The dashed, dotdashed and dotted plots are for $c = 1, 1.5, 2$ respectively. This plots bear the clear signature of thawing as one can see that for higher values of z , the statefinder r tends to 1 and the statefinder s to 0. This is because $w_X = -1$ as z increases and since in present epoch w_X deviates from -1 , r and s also deviates from 1 and 0 respectively. The same features are also observed in the cases of $n = 1.5$ and $n = 2$ in Fig. 8 and Fig. 9 respectively.

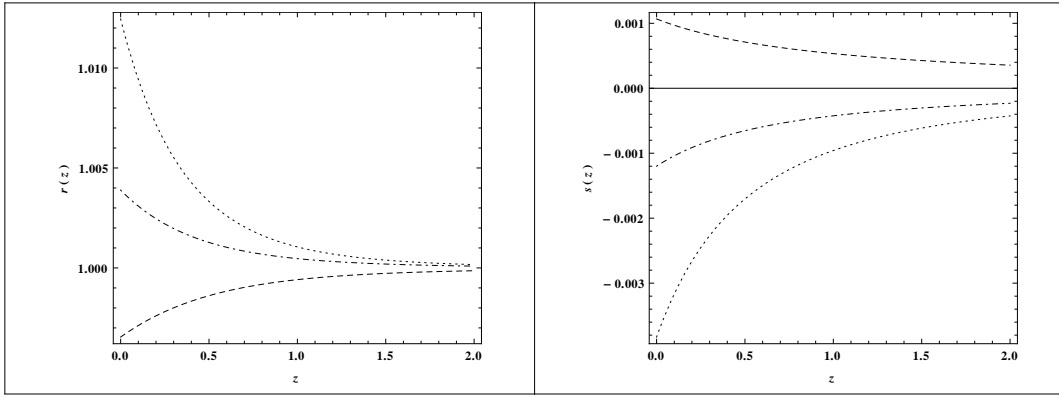


Fig. 7.— Statefinder r and s as a function of redshift z for $n=1$ and $c=1$ (dashed), 1.5 (dotdashed), 2 (dotted).

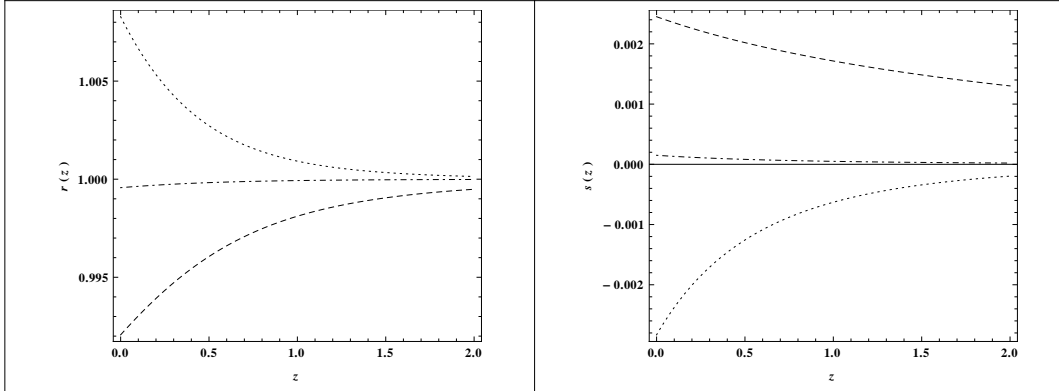


Fig. 8.— Statefinder r and s as a function of redshift z for $n=1.5$ and $c=0.5$ (dashed), 1 (dotdashed), 1.5 (dotted).

In Fig. 10, we show the variation of the $Om3$ parameters with the redshift z_3 while z_1 and z_2 are kept at $z_1 = 0.2$ and $z_2 = 0.57$. The plot at the extreme left of Fig. 10 shows this variation

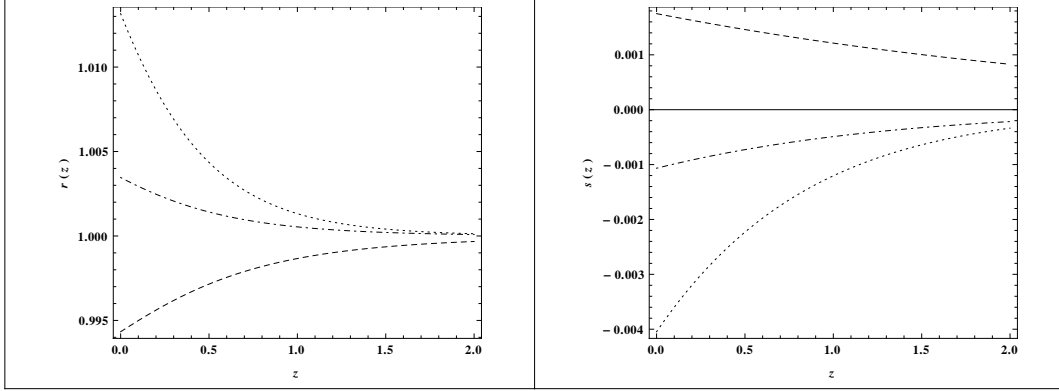


Fig. 9.— Statefinder r and s as a function of redshift z for $n=2$ and $c=0.5$ (dashed), 1 (dotdashed), 1.5 (dotted).

with $n = 1$ for $c = 1$ (dashed), $c = 1.5$ (dotdashed) and $c = 2$ (dotted). The middle and the right plots of Fig. 10 show similar variations for $n = 1.5$ and $n = 2$ respectively with $c = 0.5$ (dashed), $c = 1$ (dotdashed) and $c = 1.5$ (dotted). As $Om3$ is a three point diagnostic, we need three redshift points to measure its value. We fix two redshift points z_1 and z_2 with $z_1 = 0.2$ (Blake et al. 2011) and $z_2 = 0.57$ (Sanchez et al. 2012) and allow z_3 to be a variable. All the variation starts from a point where $z_3 = z_2$ that leaves $Om3 = 1$ and the immediate deviation of $Om3$ from 1 suggests the varying nature of dark energy which is indeed the nature of variation in thawing dark energy scenario in this case.

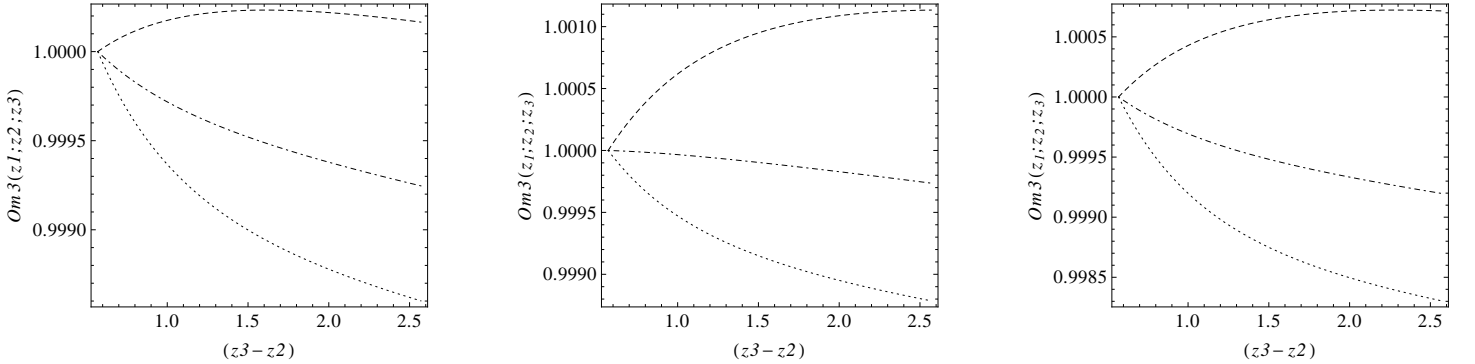


Fig. 10.— The left plot shows the variation of $Om3$ parameter as a function af redshift z_3 with $z_1 = 0.2$ and $z_2 = 0.57$ for $n = 1$ with $c = 1$ (dashed), $c = 1.5$ (dotdashed), $c = 2$ (dotted). The middle and the right plots shows the same for $n = 1.5$ and $n = 2$ respectively with $c = 0.5$ (dashed), $c = 1$ (dotdashed), $c = 1.5$ (dotted).

In Fig. 11 the average deceleration parameter q_{av} has been plotted. It is seen from the plots that all of them overlap with each other. It is thus evident that average deceleration parameter

is not capable of being a model discriminator, but it does indicate the transition period from the deceleration to acceleration phase. In this case this transition occurs between the redshift range $6.25 < z < 6.5$ as is clear from the best fit plots.

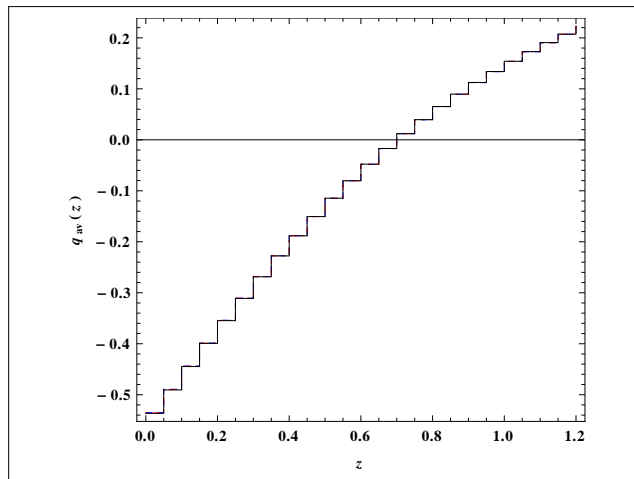


Fig. 11.— q_{av} vs z plot for $c=1$ and $n=1, 1.5, 2$.

5. Discussions and Conclusions

In this work, we proposed a two parameter generalized EOS, w_X , for thawing dark energy models and studied the dynamics of spatially flat FRW universe containing radiation, matter and dynamical dark energy. This proposal of ours is a minimal generalization of thawing dark energy EOS and is given by,

$$w'_X(a) = (1 + w_X) \frac{c}{a^n} . \quad (30)$$

This leads to $w_X(a) = -1 + (1 + w_X^0)a^c$ for $n = 1$ and for other values of n , $w_X(a) = -1 + (1 + w_X^0) \exp[\frac{c}{(n-1)}(1 - a^{(1-n)})]$, where each value of the parameters n and c defines a thawing model. Here w_X^0 is the value of w_X at the present epoch. As we have demonstrated, our model goes over the well-known thawing dark energy models such as CPL, PnGB and algebraic thawing, for suitable choice of the parameters n and c .

We have elaborately discussed the cases with $n=1$, $n=1.5$ and $n=2$ for different values of c ($c = 1, 1.5, 2$ for $n = 1$ and $c = 0.5, 1, 1.5$ for $n = 1.5, 2$). We have shown that though the parameter c is very important for the slope of the $w_X(a)$ vs. a plot, it barely changes the dynamics of the universe. This is quite evident from the average deceleration parameter ($q_{av}(z)$) vs redshift z plot (Fig. 11), growth parameter plots (Fig. 5) etc and also from the present values of matter density parameter Ω_m^0 and the Hubble parameter H_0 as well. In this context it is therefore very important to mention that fine tuning of c does not, at all, effectively change the observables like

the values of density parameters and the Hubble parameter at the present epoch (which barely suffers any change as we move from one model to another by changing the n and c values (vide Tables 2, 3 and 4). except for the variation of $w_X(a)$ with the evaluation of scale factor a of the universe. Here it is necessary to mention that in spite of treating the present epoch value of radiation density parameter Ω_r^0 as a parameter in the numerical analysis, we have chosen its value to be $\Omega_r^0 = 5.05 \times 10^{-5}$ (Beringer et al. 2012). This is because of the small value of Ω_r^0 which will not change the total density parameter upto four decimal places and therefore considering it as a parameter will not affect density parameters Ω_m^0 or Ω_X^0 upto four decimal places.

Also we would like to conclude that different values of n would lead to same cosmological dynamics for a particular value of c which is evident from average deceleration parameter plot (Fig. 11) and growth of matter perturbation plots (Fig. 5). These plots clearly demonstrate that it is hardly possible to distinguish between the results the results for different thawing models (related to different values of n and c). But the statefinder pair r, s and $Om3$ parameter can discriminate between the thawing models. These are shown in Figs. 7, 8, 9, 10.

In this context we have shown in Fig. 6 that $w_X - w'_X$ plots can, as well, serve as another discriminator of these thawing models. Nevertheless, it is shown in Fig. 6 that $w_X - w'_X$ plots are non-linear for $n = 1.5$ and $n = 2$. For the existing thawing models (e.g., PNGB and CPL cases), $w_X - w'_X$ plots are strictly linear. In a recent work, Ali et al. (Ali et al. 2009) have found this kind of nonlinear $w - w'$ plots arising from scalar field models. So our generalization can also produce them for values of n other than 1. Moreover from Fig. 6, it can be noted that as n takes higher values, only lower values of c are allowed for thawing dark energy models.

As mentioned, this is a minimal generalization with the two parameters c and n and one boundary condition given by $w_X(z = 0) = w_X^0$, z being the redshift. There may exist other generalization with more than two parameters. So selection can be made on the basis of Akaike Information Criterion (AIC) and the Bayesian Information Criterion (BIC) that are defined as,

$$AIC = -2\ln(\mathcal{L}) + 2p, \quad (31)$$

$$BIC = -2\ln(\mathcal{L}) + p \ln N, \quad (32)$$

where \mathcal{L} is the maximum likelihood value which is given by $\exp(-\chi_{min}^2/2)$, p is the number of model parameters and N is the number of data points used to find the minimum value of the χ^2 denoted by χ_{min}^2 . We show the ΔAIC and ΔBIC values in Table 5. Usually from statistical analysis, it is inferred that the models having ΔBIC in the range $0 - 2$ are strongly supported, models with $\Delta BIC > 2$ are moderately supported, and those with $\Delta BIC > 6$ are unsupported from perspective of a given data. However, in cosmology, with the rapid increase of the number of data points N (we remind the reader that we have used combined dataset), Eq (32) shows that the ΔBIC value is always going to increase with addition of a model parameter p . This does not essentially mean that the model with least number of parameters are always favored by observations, though it may appear to be so. For example, we know Λ CDM model (with the least number of parameters) (Li et al. 2010) fits the SNe Ia data only in the low redshift region i.e,

Model	ΔAIC	ΔBIC
CPL	0	0
PNGB	2	6.39
Our Model	4	12.78

Table 5: A comparative analysis of the values of Information criteria using combined χ^2 analyses of SNIa, CMB, OHD and BAO data.

for $z \ll 1$, and in this vein, most of the models pay the price just because they have additional parameters, though they, in fact fair well with observations. On this note it should be mentioned that, as demonstrated in (Parkinson et al. 2006) the above information criteria should better be replaced by Bayesian Evidence calculation, which gives a value after integrating over all probable states, and hence, does not suffer from any such limitations of AIC or BIC. Hence, nowadays, most of the cosmological models are relying more on Bayesian Evidence calculation, rather than ΔAIC or ΔBIC calculation. We hope to address this issue in near future.

Acknowledgments

We are thankful to Supernova Cosmology Project (Union 2.1) <http://supernova.lbl.gov/Union/>; Wilkinson Microwave Anisotropy Probe <http://lambda.gsfc.nasa.gov/product/map/current/> and Sloan Digital Sky Survey <http://www.sdss.org/> for providing us with the online data. We also thank S. Das and B. K. Pal for some useful comments.

REFERENCES

- Amanullah, R., et al. 2010, ApJ **716**, 712
- Ali, A., Sami, M., & Sen, A. A. 2009, PRD **79** 123501 [arXiv:0904.1070 [astro-ph.CO]].
- Ali, A., Gannouji, R., & Sami, M. 2010, PRD **82** 103012;
- Ali, A., Gannouji, R., Sami, M., & Sen, A. A. 2010, PRD **81** 104029 [arXiv:1001.5384 [astro-ph.CO]].
- Abraham, R. G., et al. 2004, AJ **127** 2455.
- Beringer, J., et al. 2012, [Particle Data Group Collaboration], PRD **86** 010001
- Bento, M. d. C., Bertolami, O., & Sen, A. A. 2003, PRD **67** 063003 [astro-ph/0210468];

- Blake, C., et al. 2011, MNRAS **418**, 1707
- Caldwell, R. R., & Linder 2005, E. V. 2005, PRL **95**, 141301.
- Chen, S. H., et al. 2011, PRD **83** 023508;
- Chen, X., et al. 2011, PLB **695**, 30;
- Chevallier, M., & Polarski, D. 2001, IJMPD **10**, 213 [gr-qc/0009008].
- Chiba, T., Dutta, S., & Scherrer, R. J. 2009, PRD **80**, 043517 [arXiv:0906.0628 [astro-ph.CO]];
- da Conceicao Bento, M., Bertolami, O., Santos, N. M. C., & Sen, A. A. 2006, JPCS **33**, 197 [astro-ph/0512076];
- Das, S., Ghosh, S., van Holten, J. W., & Pal, S. 2011, IJMPD **20**, 1235 [arXiv:0906.1044 [astro-ph.CO]].
- Davis, T. M., et al. 2007, ApJ **666**, 716
- Dutta, K., & Sorbo, L. 2007, PRD **75**, 063514 [astro-ph/0612457].
- Dutta, S., & Scherrer, R. J. 2011, PLB **704**, 265 [arXiv:1106.0012 [astro-ph.CO]];
- Dutta, S., & Scherrer, R. J. 2010, PRD **82**, 043526 [arXiv:1004.3295 [astro-ph.CO]];
- Dutta, S., Saridakis, E. N., & Scherrer, R. J. 2009, PRD **79**, 103005 [arXiv:0903.3412 [astro-ph.CO]];
- Dutta, S., & Scherrer, R. J. 2009, PLB **676**, 12 [arXiv:0902.1004 [astro-ph.CO]].
- Frieman, J. A., Hill, C. T., Stebbins, A., & Waga, I. 1995, PRL **75**, 2077 [astro-ph/9505060];
- Gaztañaga, E., Cabré, A., Hui, L. 2009, MNRAS **399**, 1663 (G09);
- Gupta, G., Saridakis, E. N., & Sen, A. A. 2009, PRD **79**, 123013 [arXiv:0905.2348 [astro-ph.CO]];
- Harko, T., Lobo, F. S. N. 2010, EPJC **70**, 373.
- Hirano K., Komiya Z. 2011, IJMPD **20**, 1;
- Huang Z. G., Lu H. Q. & Zhang K. 2011, ApSS **331**, 331 [arXiv:1005.0433 [astro-ph.CO]].
- Jimenez, R., & Loeb, A. 2002, ApJ **573**, 37;
- Kaloper, N., & Sorbo, L. 2006, JCAP **0604**, 007 [astro-ph/0511543];
- Kessler, R., et al. 2009, ApJS **185** , 32
- Komatsu, E., et al. 2009, ApJS 180, 330;

- Komatsu, E., et al. 2011, ApJS **192**, 18.
- Kowalski, M., et al. . 2008, ApJ **686**, 749
- Kujat, J., Scherrer, R. J., & Sen, A. A. 2006, PRD **74**, 083501 [astro-ph/0606735];
- Li, M., Li, X., & Zhang, X. 2010, SCPMA **53**, 1631 [arXiv:0912.3988 [astro-ph.CO]].
- Li, X. z., Sun, C. b., & Xi, P. 2009, JCAP **0904**, 015 [arXiv:0903.4724 [gr-qc]].
- Linder, E. V. 2008, GRG **40**, 329 [arXiv:0704.2064 [astro-ph]].
- Linder, E. V. 2003, PRL **90**, 091301 [astro-ph/0208512].
- Lu, J., Xu, L., Chang, B., & Gui, Y. 2009, IJMPD **18**, 1741 [arXiv:0812.2074 [astro-ph]].
- Nesseris, S., & Shafieloo, A. 2010, MNRAS **408**, 1879 [arXiv:1004.0960 [astro-ph.CO]].
- Novosyadlyj, B., et al. 2010, PRD **82**, 103008;
- Panotopoulos, G. 2008, NPB **796**, 66 [arXiv:0712.1177 [astro-ph]].
- Parkinson, D., Mukherjee, P., & Liddle, A. R. 2006 Phys.Rev. **D73**, 123523.
- Perlmutter, S., et al. 1999, ApJ **517**, 565;
- Percival, W. J., et al. 2010, MNRAS **401**, 2148;
- Podariu, S., et al. 2001, ApJ **559**, 9;
- Ratra, B., et al. 1999, ApJ **517**, 549;
- Riess, A. G., et al. 1998, AJ **116**, 1009
- Riess, A. G., et al. . 2007, ApJ **659**, 98
- Riess, A. G., et al. 2009, ApJ **699**, 539
- Rosenfeld, R., & Frieman, J. A. 2007 2007, PRD **75**, 043513 [astro-ph/0611241];
- Sahni, V., Shafieloo, A., & Starobinsky, A. A. 2008, PRD **78**, 103502 [arXiv:0807.3548 [astro-ph]].
- Sahni, V., Saini, T. D., Starobinsky, A. A., & Alam, U. 2003, JETPL **77**, 201 [PZETF **77** (2003) 249] [astro-ph/0201498].
- Sanchez, A. G., Scoccola, C. G., Ross, A. J., Percival, W., Manera, M., Montesano, F., Mazzalay, X., & Cuesta, A. J., et al. 2012, arXiv:1203.6616 [astro-ph.CO];
- Samushia, L., Ratra, B. 2009, APJ **701**, 1373;

- Sen, S., Sen, A. A., & Sami, M. 2010, PLB **686**, 1 [arXiv:0907.2814 [astro-ph.CO]];
- Shafieloo, A., & Clarkson, C. 2010, PRD **81**, 083537 [arXiv:0911.4858 [astro-ph.CO]].
- Shafieloo, A., Sahni, V., & Starobinsky, A. A. 2008, arXiv:1205.2870 [astro-ph.CO].
- Scherrer, R. J., & Sen, A. A. 2008, PRD **78**, 067303 [arXiv:0808.1880 [astro-ph]];
- Scherrer, R. J., & Sen, A. A. 2008, PRD **77**, 083515 [arXiv:0712.3450 [astro-ph]];
- Simon, J., Verde, L., & Jimenez, R. 2005, PRD **71** 123001. 93.
- Suzuki, N., Rubin, D., Lidman, C., Aldering, G., Amanullah, R., Barbary, K., Barrientos, L. F., & Botyanszki, J., et al. 2012, ApJ **746**, 85 [arXiv:1105.3470 [astro-ph.CO]].
- Tsujikawa, S. 2010, arXiv:1004.1493 [astro-ph.CO].
- Wang, L. M., & Steinhardt, P. J. 1998, ApJ **508**, 483 [astro-ph/9804015].
- Wood-Vasey, W. M., et al. 2007, ApJ **666**, 694
- Zhang, C., Zhang, H., Yuan, S., Zhang, T. J., & Sun, Y. C. 2012, arXiv:1207.4541 [astro-ph.CO];